AD-750 364

MEASUREMENT OF THE ANGULAR DISTRIBUTION OF PHOTOELECTRONS FROM THIRD GENERATION PHOTOCATHODE MATERIALS

John H. Pollard

Army Electronics Command
Fort Belvoir, Virginia

1972

DISTRIBUTED BY:

NTIS
National Technical Information Service
U. S. DEPARTMENT OF COMMERCE
5285 Port Royal Road, Springfield Va. 22151

AD 750 364

Details of illustrations in this document may be better studied on microfiche.

MEASUREMENT OF THE ANGULAR DISTRIBUTION OF PHOTOELECTRONS FROM THIRD GENERATION PHOTOCATHODE MATERIALS (U)

DDC RECEIVED NOV 27 1972

JOHN H. POLLARD
NIGHT VISION LABORATORY
FORT BELVOIR, VIRGINIA

INTRODUCTION

A great deal of work has been reported on the photoemissive properties of semiconductors exhibiting negative electron affinity following the discovery in 1965 by Scheer and Van Laar (1) of efficient photoemission from GaAs. A recent review of the present development of III-V semiconductor photocathodes has been given by Bell and Spicer (2). Despite the practical importance of the spacial distribution of the photoemitted electrons from III-V semiconductors, the photocathodes for use in third generation image intensifiers, surprisingly little work has been reported on this property. Theoretical interest in angular measurements for further understanding of photoemission (3,6) has resulted in some measurements for clean GaAs by Wooten et.al. (4) and preliminary results for a negative electron affinity GaAs(100) surface (5). The latter showed an extremely narrow distribution, Gaussian, in angle, about the surface normal for the photoemission. This surprising result contrasts with the angular distribution for clean semiconductors which is expected to approximate a Lambertian distribution from Kanes' theory (6). In a study of conventional photocathodes, which are known to be semiconductors (7), Burns (8,9) has obtained angular distributions which approximate a Lambertian form. This paper confirms the surprisingly narrow distribution for other surfaces of GaAs and a mathematical model is presented to explain the observations. A result of the analysis shows that a narrow emission cone is expected for all III-V semiconductors which can be activated to negative electron affinity. It is expected that third generation photocathodes will show significant improvements in resolution capability, for proximity focused devices, over conventional photocathodes.

2. EXPERIMENTAL DETAILS

A schematic diagram of the apparatus is shown in Figure 1 which was essentially a Varian 240 LEED/Auger ultra high vacuum system. The low energy electron diffraction (LEED) gun was of the off-axis type

This document has been approved for public release and sale; its distribution is unlimited.

Reproduced by
NATIONAL TECHNICAL INFORMATION SERVICE
U S Department of Commerce
Springfield VA 22151

and the crystal sample could be illuminated with light from a Bausch and Lomb, high intensity monochromator, directly through a sapphire window and the gun electrode structure, allowing visual display of the photoemission on the LEED phosphor screen. The crystal specimen was mounted in the holder, Figure 2a, furnished with an indirect heater for heat cleaning purposes. Cesiations were performed from a cesium molecular source, sealable to ultra high vacuum (10), operating at room temperature, with line of sight to the sample. The two degrees of rotational freedom and the geometrical arrangement was designed to allow the photoemission replenishment crystal current under illumination from the monochromator to be monitored during activation. Oxygen was admitted by a Varian leak valve into the main LEED chamber from a separate gas handling section supplied in turn from a liter flask of high purity oxygen (10ppm Kr and 2ppm Xe the only detectable impurities). Ambient background vacuum conditions, which was $\sim 2 \times 10^{-10}$ torr, and the gas purity were monitored with an EAI quadropole mass spectrometer. Residual magnetic fields were nulled out by three sets of mutually perpendicular Helmholtz coils and was accomplished by observations of the LEED pattern from the GaAs(100) surface. After final nulling the (00) spot position remained fixed throughout the range 1-300 volts. The ($\frac{1}{2}$,0), (0,0) and ($-\frac{1}{2}$,0) spots were observed at 6 volts beam energy and the pattern was symmetrical after centering the (0,0) beam indicating the absence of magnetic and electrostatic fields and of focussing effects at low energy.

Three crystal surfaces have been measured, GaAs(100), GaAs(111)B, and GaAs(110). The crystals were Zn doped $\sim 1 \times 10^{19} cm^{-3}$; the first two were vapor grown 10 micron films on a GaAs substrate, supplied by D. Pommerrenig, Night Vision Laboratory, while the latter was cleaved from bulk Monsanto material. Auger spectroscopy measurements were used to identify surface impurities, carbon and oxygen. The surfaces were ion bombarded to remove carbon and removal of the residual oxygen was monitored while heating. A temperature of approximately 600°C was necessary to remove the last traces of oxygen. The LEED patterns obtained from the three surfaces after cleaning were similar to earlier work reported by Macrae and Gobeli (11) for the (110) surface and by Jona (12) for the (100) and the (111)B surfaces. The (110) surface gave a 1x1 pattern, the (100) surface a 2x8 pattern and the (111)B surface did not show any ordered pattern. Prolonged heating at 600°C caused faceting of the (100) and (111)B surfaces to (110) facets and care was taken to avoid this for the surfaces reported in this paper. Activation sensitivities were in the range ~500 μA/lumen for the three specimens.

The crystal specimen was illuminated with a light beam 2 mms. in diameter and after optimum activation, using the familar "Yo-Yo" technique with cesium and oxygen, to maximize the photoresponse, the photoelectrons were post accelerated for display on the phosphor screen in the conventional LEED method. It was necessary to bias the crystal ~10 volts negative relative to the first grid; all four

grids were biased to the same relative potential by direct observation of the photoemission display. The photoemission was cylindrically symmetric about the surface normal Figure 2d and quantitative measurements of the intensity distribution with angle was obtained with a spot photometer measurement of the phosphor intensity. The photometer measured an area equivalent to an angle of 1·5° subtended at the crystal and represents the resolution of each individual measurement. Actual data points for the angular distributions were obtained every 2° and were taken by rotating the crystal and monitoring one fixed spot on the phosphor. The photoemission was insensitive to the direction of the incident light for the small range of incident angles necessary to take the measurements.

Electron energy distributions have been taken for the three surfaces and the results for the GaAs(110) surface are presented. The measurements were taken by an a.c. differentiation technique similar to that used in Auger spectroscopy. A small a.c. signal ~20 millivolts was supplied to the center two grids of the four grids of the LEED unit which was ramped to sweep through the energy region of photoemission. Synchronous detection of the current to the phosphor allowed a direct read out of the photoemission energy distribution. We obtained resolutions of ~0·1eV for the distribution and have confirmed, by measuring individual grid and crystal currents that 95% of the photoemitted electrons were analyzed by the π solid angle of the LEED unit.

3. ANGULAR MEASUREMENT OF THE PHOTOEMISSION

Photographs of the photoemission were obtained for the activated GaAs(100) surface for white light illumination. These are shown for two different orientations of the crystal in Figure 2d and Figure 2e. The reflected light beam from the crystal can be observed on the grid structure and phosphor of the LEED unit in these photographs. The photoemitted electrons approximately bisect the incident and reflected light directions providing evidence for cylindrical symmetry of the emission about the surface normal. An over exposed photograph of the distribution Figure 2f illustrates that electrons are emitted only into a well directed cone, substantiated by the absence of background intensity (the camera angle was chosen to eliminate the light beam reflections). The crystal orientation was set to give photoemission in the direction shown in Figure 2e and the spot photometer was aligned on the center of the display. The crystal was then rotated to obtain the angular distribution (this particular orientation avoided measuring the reflected light beam in the spot photometer).

Measurements for the activated GaAs(100) surface in the wavelength range 900-350 mμ are shown plotted in Figure 3. Different diffraction gratings were used to take the measurements for the 900-700 mμ and the 750-350 mμ regions of the spectrum and the corresponding results have been separated in the plots for clarity. No attempt

has been made to normalize the results because the distributions were essentially independent of the light intensity. Figures 4 and 5 show corresponding measurements for activated GaAs(111)B and GaAs (110) surfaces, respectively.

Detailed inspection of these results show that the distributions are Gaussian, in angle, about the surface normal with a half width at half maximum (HWHM) intensity which is wavelength dependent varying from $\sim 5^{\circ}$ at 850 mμ to $\sim 9^{\circ}$ at 350 mμ and which is approximately the same for all three surface orientations. The results are summarized in Figure 8. Differences in cone angle for the (100) and (110) surfaces with the different monochromators resulted from changes in sensitivity of the specimen, however, in all cases, the highest sensitivity corresponded to the smallest cone angle.

4. MATHEMATIC MODEL

We consider the emission of an electron, energy E above the band edge of GaAs, diffusing from position 1 Figure 6 into the band bending acceleration region. At position 2 the electron energy has increased by ½kT and we make the assumption that the equilibrium distribution at this point is the same as at position 1 shifted in energy but such that $K_p = K_p'$. (K_n and K_p are the components of momentum normal and parallel to the surface). This assumption is necessary because the transport through the 'thermal' part of the band bending region (shaded portion) is rather slow. Subsequent acceleration to position 3 is rapid and there is insufficient time for scattering events to occur, consequently, momentum parallel to the surface is conserved giving $K_p'' = K_p' = K_p$. Calculations of the transit time in the band bending region (5) based on a 'Schottky layer' model for the space charge region and the known band structure of GaAs (13) suggest this is reasonable. The transit time for 1×10^{19} doping is $\sim 2\times10^{-14}$ seconds considerably faster than acoustical or polar optical scattering times $\sim 10^{-12}$ secs. Intervalley $\Gamma_1 - X_1$ scattering times are $\sim 10^{-13}$ secs. for GaAs from work of James and Moll (14) for energies 0.3eV above the band edge, however, a thermalized Γ electron only has energy > 0.3eV above the band edge for $\sim 2\times10^{-15}$ secs. before emission and this process is thus insignificant. We make the further assumptions that no scattering occurs in the activation layer and that the surface is specularly reflecting. Momentum parallel to the surface is conserved giving at position 4 and 5 $K_{po} = K_p''' = K_p''$. Electrons reflected at the surface by analogy with the above process return to the diffusion region, these will not concern us here. We assume a constant escape probability in the following analysis. Energy conservation requires:

$$E = \frac{\hbar^2}{2m^*}\,(K_n^2 + K_p^2) \text{ and } E + E_A = \frac{\hbar^2}{2m}\,(K_{no}^2 + K_{po}^2) \qquad [1]$$

where m^* is the effective mass associated with the Γ_1 region of the conduction band and m is the free electron mass. We consider electrons emitted along a conical surface of semiangle θ about the surface normal, whence:

$$\mathrm{Tan}\theta = K_{po}/K_{no} = K_p/K_{no} \qquad [2]$$

Combining Equations 1 and 2 gives:

$$K_n^2 = K_p^2\left(\frac{m^*}{m}\mathrm{Cosec}^2\theta - 1\right) - \frac{2m^*}{\hbar^2}E_A \qquad [3]$$

for all electronsemitted at angle θ to the surface normal.

We now consider the equilibrium conditions in the diffusion region of the GaAs in order to ascertain the number of electrons satisfying Equation 3. We assume spherical energy bands in K-space centered at Γ_1 for GaAs, Figure 7, and consider only the Γ_1 region of the band. The number of states between $K_n \rightarrow K_n + \delta K_n$ and $K_p \rightarrow K_p + \delta K_p$ in a solid of volume V (15), is

$$\delta n = (V/8\pi^3)\cdot 2\pi K_p \cdot \delta K_p \cdot \delta K_n \qquad [4]$$

A thermalized distribution of electrons in the conduction band obeys Fermi-Dirac statistics and can be approximated by a Boltzman distribution with occupation probability $\propto \exp -E/kT$ for energy E above the band edge. Combining this with Equation 4:

$$\delta n_o = A\cdot\exp\left(-\frac{\hbar^2}{2m^*kT}\left(K_n^2 + K_p^2\right)\right)\delta(K_p^2)\cdot\delta K_n \qquad [5]$$

where A is a normalizing constant and δn_o is the number of occupied states. Substituting for K_n from Equation 3 in Equation 5 and integrating gives:

$$N = A\int_0^{\theta}\int_{K_p}^{\infty}\phi(K_p,\theta)\exp\left(-\frac{\hbar^2}{2mkT}K_p^2\mathrm{Cosec}^2\theta + \frac{E_A}{kT}\right)\cdot\delta(K_p^2)\cdot\delta\theta \qquad [6]$$

where N is the total number of electrons contained in a cone of semiangle θ and the lower limit on K_p is determined from Equation 3 with $K_n^2 = 0$. The function $\phi(K_p,\theta)$ is given by:

$$\phi(K_p,\theta) = \frac{K_p^2\,\frac{m}{m^*}\mathrm{Cosec}^2\theta\cdot\mathrm{Cot}\theta}{\left(K_p^2\left(\frac{m^*}{m}\mathrm{Cosec}^2\theta - 1\right) - \frac{2m^*}{\hbar^2}E_A\right)^{1/2}}$$

The differential yield δY; (number of electrons emitted/unit solid angle) at any angle θ, is given by:

$$\delta Y = \left(\frac{\delta N}{\delta\theta}\right)\cdot\delta\theta/2\pi\mathrm{Sin}\theta\cdot\delta\theta \qquad [7]$$

From Equation 6 we have:

$$\delta Y = \frac{A\ \exp\left(\frac{E_A}{kT}\right)}{2\pi \mathrm{Sin}\theta} \int_{K_p}^{\infty} \phi(K_p,\theta)\cdot\exp\left(-\frac{\hbar^2}{2mkT} K_p{}^2 \mathrm{Cosec}^2\theta\right)(\delta K_p{}^2) \qquad [8]$$

Integrating Equation 8, after some tedious algebra, gives:

$$\delta Y = \frac{A}{2\pi^{\frac{1}{2}}} \left(\frac{m}{m^*}\right) \left(\frac{2m^*kT}{\hbar^2}\right)^{3/2} \left[\frac{2E_A}{kT}\left(1-\frac{m}{m^*}\mathrm{Sin}^2\theta\right)^{-3/2} + \left(1-\frac{m}{m^*}\mathrm{Sin}^2\theta\right)^{-\frac{1}{2}}\right]$$

$$\times\ \mathrm{Cos}\theta\cdot\exp\left(-\frac{E_A}{kT}\left(\frac{\frac{m}{m^*}\mathrm{Sin}^2\theta}{1-\frac{m}{m^*}\mathrm{Sin}^2\theta}\right)\right) \qquad [9]$$

The spacial distribution is essentially contained in the exponential term and the HWHM semicone angle $\theta_{\frac{1}{2}}$, is given by:

$$\mathrm{Sin}^2\theta_{\frac{1}{2}} = \frac{m^*}{m}\left(\frac{kT}{1\cdot45E_A + kT}\right) \qquad [10]$$

The angle $\theta_{\frac{1}{2}}$ depends on m^*, the effective mass, E_A, the negative electron affinity and kT, the 'effective temperature' of the distribution. The Gaussian form of the distribution depends on achieving a negative electron affinity where $E_A > kT$ and approximates $\exp - E_A/kT\ (m/m^*)\cdot\theta^2$. The small angle, observed in the case of GaAs, results from the small effective mass associated with the Γ_1 minimum. It should be noted that the above arguments are independent of the surface orientation, in agreement with the experimental observations.

Electron energy distribution for the GaAs(110) surface are shown in Figure 9 for different wavelengths. The width of the distribution, which provides a measure of the 'effective temperature' of the emitted electrons, is essentially constant between 900-750 mμ and increases at shorter wavelengths. We associate, therefore, effective temperatures of 0.025eV with 850 mμ and 0.05eV with 400 mμ and substituting in Equation 10 gives HWHM values for the angular distributions in agreement with Figure 8. The energy distributions (Figure 9) disagree with work of Eden (16) and others, who obtain separate Γ and X peaks, 0.3 volts apart, at wavelengths shorter than 6,500°A. Pierce and De Stephano (17) have analyzed the cylindrical geometry used by Eden et.al. for energy distribution measurements and show that good resolution can be obtained for electron emission obeying a Lambertian angular distribution. As we have shown the emission is very directional for GaAs and field effects at the entrance aperture, necessary to admit light, could become most important and may be the

origin of the differences between the distributions. Considerations of the band structure (5) of GaAs shows that, for reasonable values of band bending ~1.0eV, electrons transported in the X minimum will be Bragg reflected before reaching the surface. Only electrons that are scattered in the band bending region, therefore, can escape, representing a small fraction of electrons thermalized in the X minimum. This is in qualitative agreement with our measured energy distributions.

5. DISCUSSION

The experimental measurements of the angular distribution of photoemitted electrons from cesium-oxygen activated p-type GaAs surfaces shows a highly directional photoemission approximately independent of the surface orientation. The mathematical model explaining these observations shows the expected Lambertian distribution is modulated by a strong exponential function resulting from the attainment of negative electron affinity conditions. The exponential function is a Gaussian distribution in Sinθ, for conditions where $E_A > kT$; in the case of a small effective mass associated with the thermalized distribution in the solid, Sinθ may be replaced by θ, and the distribution is Gaussian, in angle, about the surface normal. This is the case for GaAs. Similar considerations can be applied to other III-V compounds and Table 1 shows the effective mass values and the bandgap energy for binary compounds. Clearly in all cases where the bandgap is less than 1.5eV the effective mass is < 0.1 and for these materials we may expect to find similar directional properties for the photoemission, provided negative electron affinity conditions can be achieved. The argument can be extended to the new ternary materials GaInAs, InAsP, GaAsSb under consideration for extended infrared response photocathodes (2). The angular spread of the photoelectrons is wavelength dependent but in the case of GaAs remains essentially unchanged throughout the range 900-700 mμ, the practically useful region in infrared applications.

In summary, it is expected that highly directional photoemission will be characteristic of all photocathodes used in third generation image intensifiers. In Figure 10 we have compared the directional properties of GaAs with conventional photocathodes in polar plots of the differential yield. The directionality of emission from GaAs is strikingly illustrated and this can be expected to offer important advantages in wafer tube technology. In any proximity focussed device greatly improved resolution can be obtained; typically, a tube with 60 mil cathode to first tube element spacing operating at 6Kv has a resolution ~40 lp/mm for a conventional photocathode, under the same operating conditions 400 lp/mm resolution is potentially available by changing the cathode to GaAs. It should be cautioned that such high resolution has not been observed in diode structures (18); other factors presently limit the resolution capability of GaAs (19). Nonetheless, we believe high resolution is obtainable from the use of III-V semiconductor photocathodes in proximity focussed devices.

6. ACKNOWLEDGEMENTS

It is a pleasure to acknowledge the technical skill of J. Kovals in designing accessories for the LEED unit and to many of my colleagues at Night Vision Laboratory, for stimulating discussions on many aspects of this work.

REFERENCES

1. J. J. Scheer and J. van Laar, Solid State Comm. 3, 189, 1965.
2. R. L. Bell and W. E. Spicer, Proc. IEEE, 58, 11, 1788, 1970.
3. G. D. Mahan, Phys Rev B. 2, 11, 4334, 1970.
4. F.Wooten,T.Huen and H. V. Winsor, Phys. Letters, 36A, 351, 1971.
5. J. H. Pollard, Paper C.4. Conference on Photoelectric and Secondary Electron Emission, University of Minnesota, August 71.
6. E. O. Kane, Phys Rev 127, 1, 131, 1962.
7. A. H. Sommer, Photoemissive Materials, John Wiley and Sons, 1968.
8. J. Burns, Final Report, Contract No. DA-44-009-ENG-5004, May 1965
9. J. Burns, Final Report, Contract No. DA-44-009-AMC-938(T),Feb 69.
10. J. H. Pollard, J. Kovals and K. H. Kaldenback, Patent Pending.
11. A. U. MacRae and G. W. Gobeli, Jour. Appl. Phys. 35, 5, 1629,1964
12. F. Jona, IBM Jour. Res. Dev. 9. 5-6, 375. 1965.
13. F. Herman, quoted by L. W. James, Stanford Electronics Laboratories, Tech Report 5221-2, U.S. Army Contract No. DA-44-009-AMC-1474 and Center for Materials Research Contract SD-87.
14. L. W. James and J. L. Moll, Phys. Rev. 183, 3, 740. 1969.
15. J. M. Ziman, Principles of the Theory of Solids - Cambridge University Press, Chapter 3, 1965.
16. R. C. Eden, PhD Thesis, Stanford University, 1967.
17. T. H. DiStephano and D. T. Pierce, Rev. Sci. Inst. 41, 2, 180 1970.
18. L. V. Caldwell and A. J. Kennedy, Paper C.5. Conference on Photoelectric and Secondary Electron Emission, University of Minnesota, August 1971.
19. N. Diakides and C. M. Thomas, private communications.

FIGURE CAPTIONS

Figure 1 Schematic diagram of the LEED/Auger system

Figure 2 (a) A view of the specimen holder with crystal mounted.
(b) LEED pattern at 40V for GaAs(100) surface-(2x8) pattern.
(c) LEED pattern at 78V for GaAs(100) surface-(2x8) pattern.
(d) Spacial Distribution of Photoelectrons-(crystal rotated 45° in azimuth) for white light illumination (note reflected light beam from the grids).
(e) Spacial Distribution of Photoelectrons (0° azimuth) for white light illumination.
(f) Overexposure of (e).

Figure 3 Plots of the measured angular distribution for GaAs(100) for the ranges 900-700 mμ and 750-350 mμ (different monochromators were used in each range). The distributions can be very accurately fit by a Gaussian distribution, in angle, about the surface normal, indicated by 0° on the absissa.

Figure 4 Identical plot to Figure 3 for the GaAs(111)B surface.

Figure 5 Identical plot to Figure 3 for the GaAs(110) surface.

Figure 6 The band diagram for activated GaAs in the band bending region showing the appropriate momentum conditions for the transport of a thermalized electron from the diffusion region into vacuum. The lightly shaded region indicates the 'thermal' part of the band bending region.

Figure 7 Spherical energy contours in K-space and its relation to the direction momentum components K_p, K_n.

Figure 8 Plots of the variation of HWHM of the angular distribution with wavelength for GaAs(100), (110) and (111)B Surfaces. The 900-700 mμ monochromator readings are shown with full circles and 750-350 mμ monochromator readings with open circles. Values of the electron affinity shown for each surface were deduced from the HWHM values at 800 mμ using Equation 10, Section 4, and assuming kT = 0.025eV and m* = 0.07.

Figure 9 Electron energy distributions as a function of wavelength for the GaAs(110) surface. The band edge is estimated to be at 0.22eV on the energy scale. The instrumental resolution is estimated to be 0.1eV. The distributions do not show separate Γ_1 and X_1 peaks as found by Eden (16).

Figure 10 A comparison of the polar plots of the differential yield for GaAs with a Lambertian distribution, S-1, and Cs_3Sb photocathodes. The radius vector from the origin to the individual curves in any direction is proportional to the electron intensity in that direction. The shaded lines indicate the plane of the cathode surface.

TABLE

Table 1 A compilation of effective mass values associated with Γ_1 and the bandgap energy for III-V binary semiconductors.

TABLE 1

BANDGAP / m*(Γ_1)	P	As	Sb
A1	2.5 / -	2.3 / -	1.65 / 0.30
Ga	2.25 / 0.13	1.42 / 0.07	0.68 / 0.05
In	1.32 / 0.07	0.33 / 0.03	0.23 / 0.01

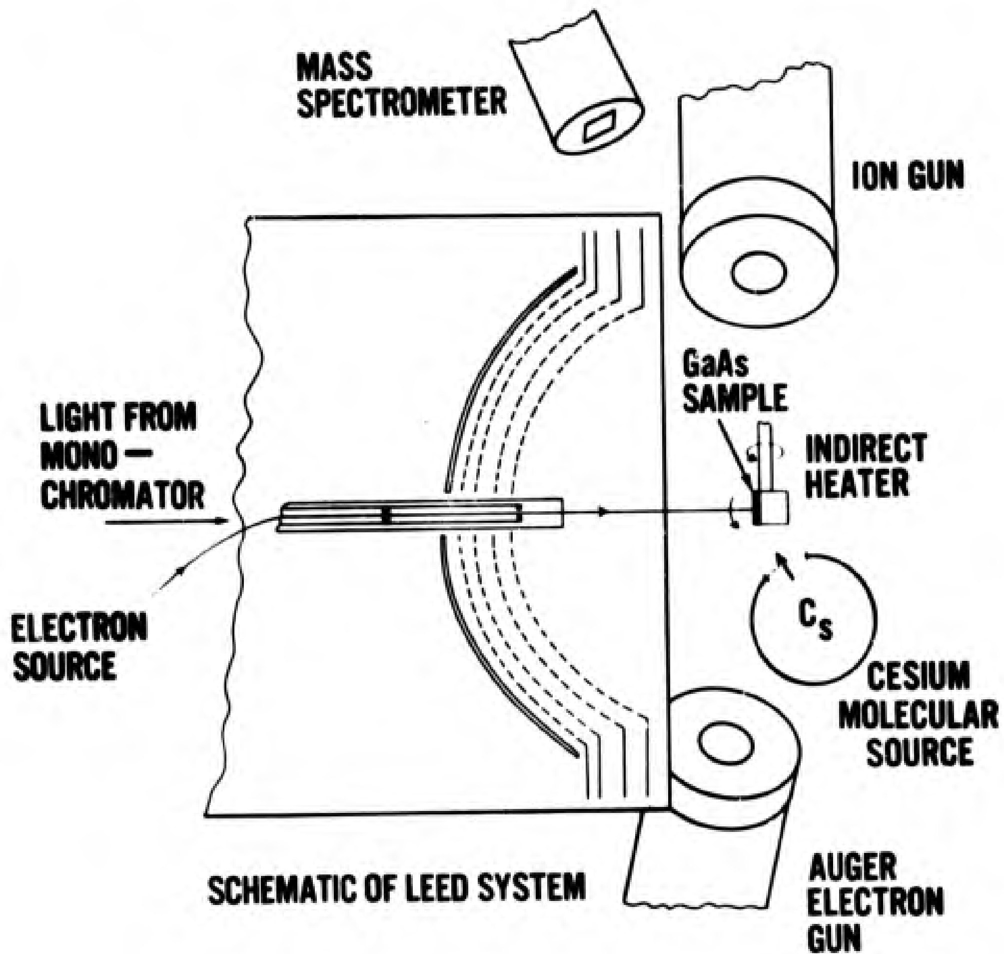

FIG. 1

Reproduced from best available copy.

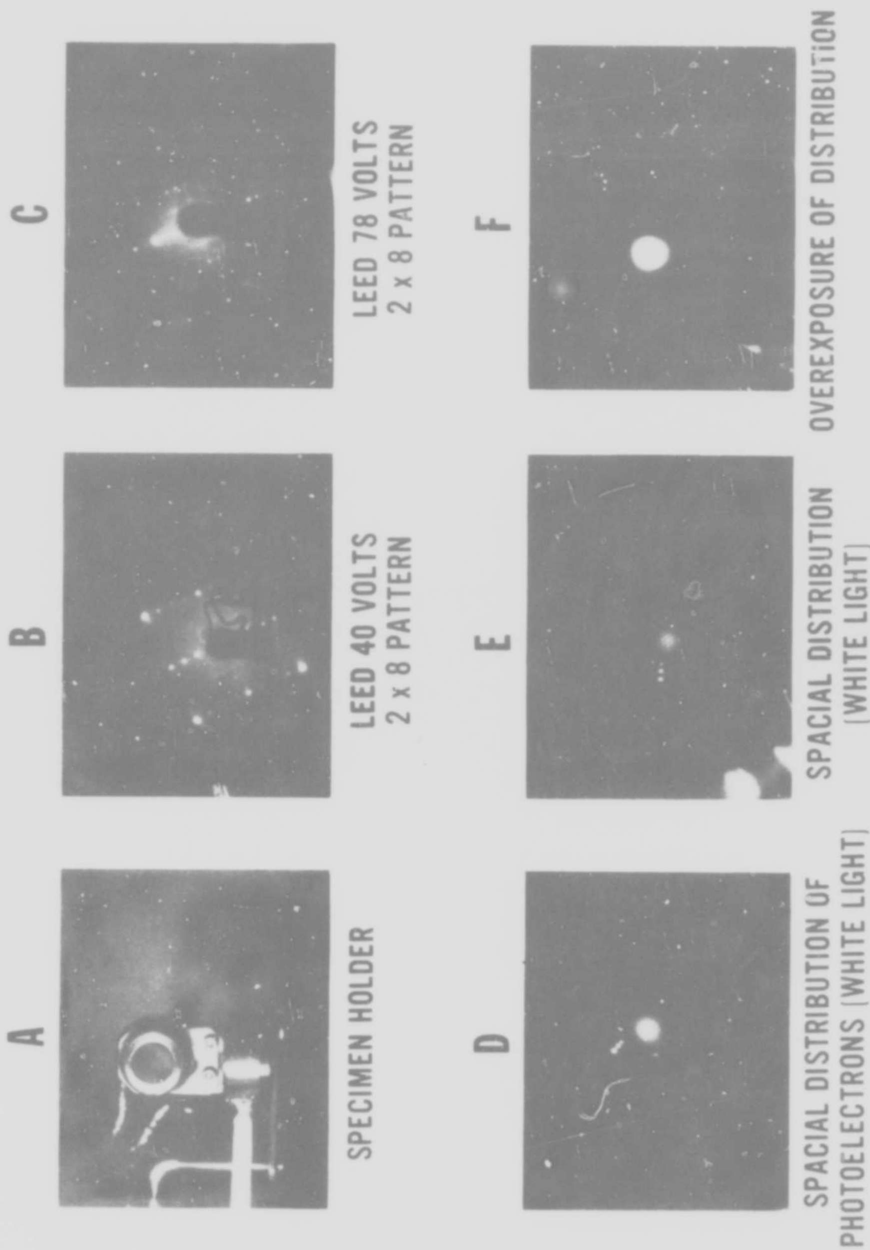

Fig. 2

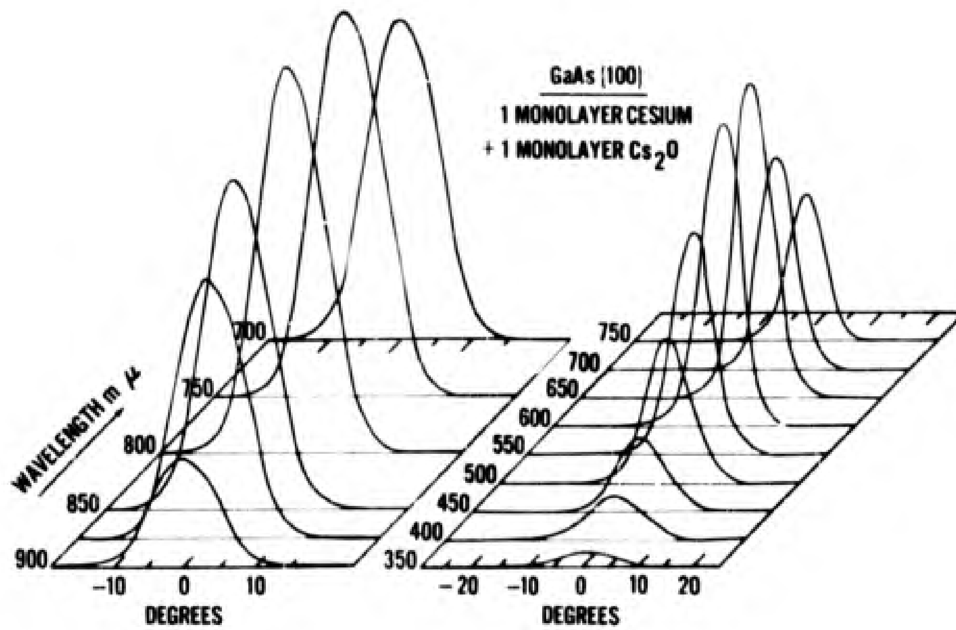

FIG. 3

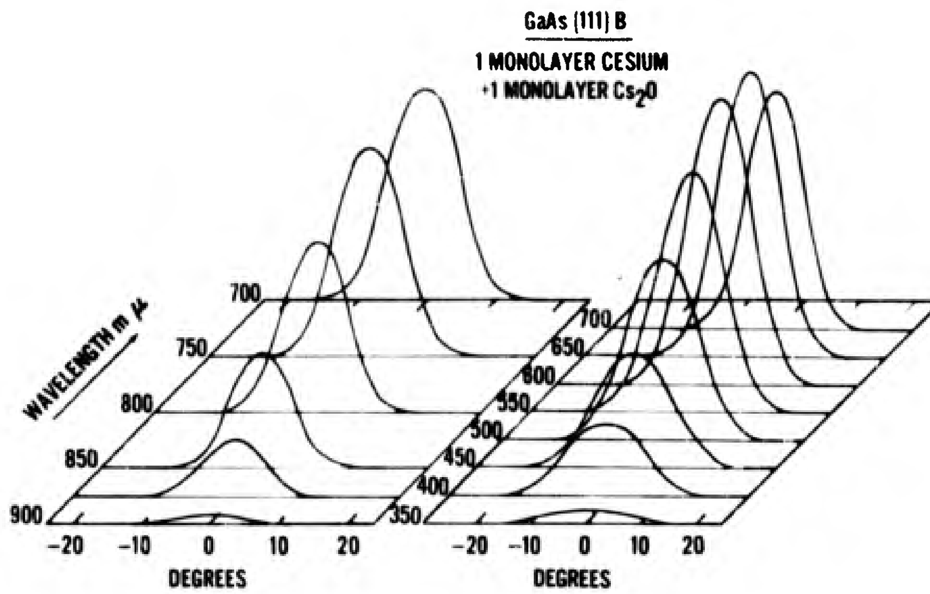

FIG. 4

FIG. 5

FIG. 6

FIG. 7

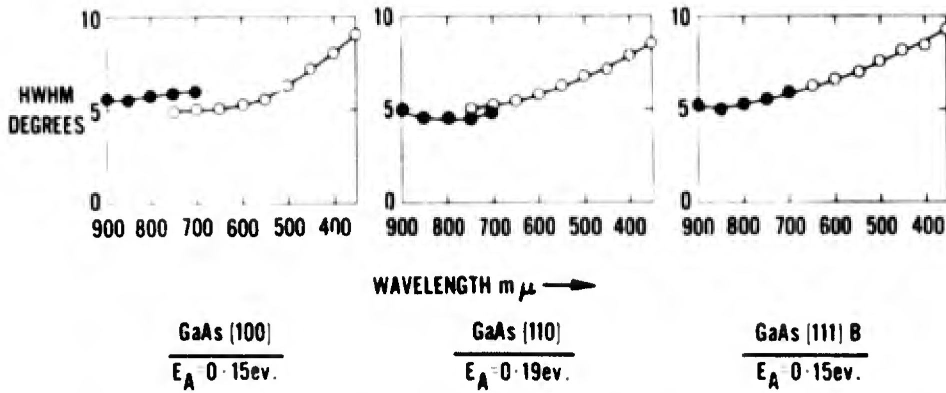

FIG. 8

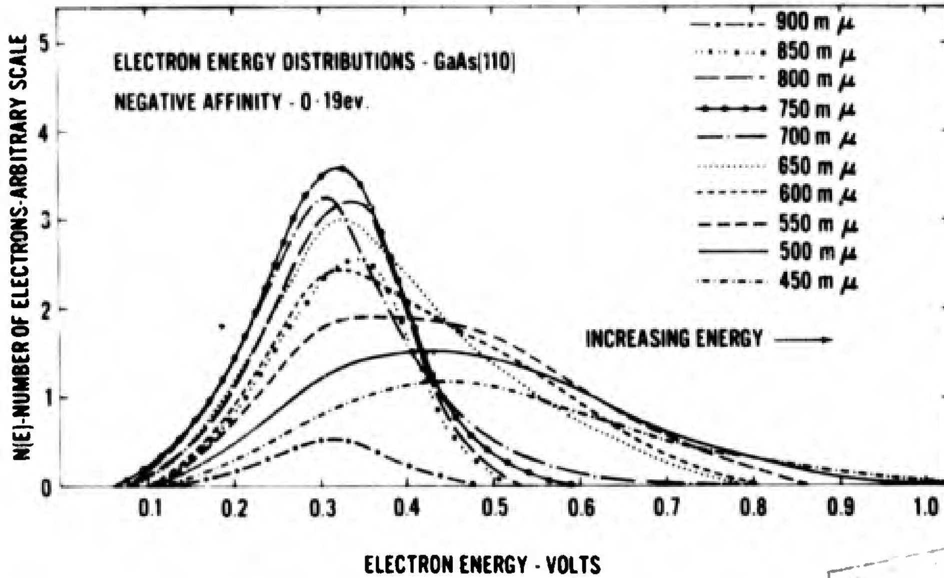

FIG. 9

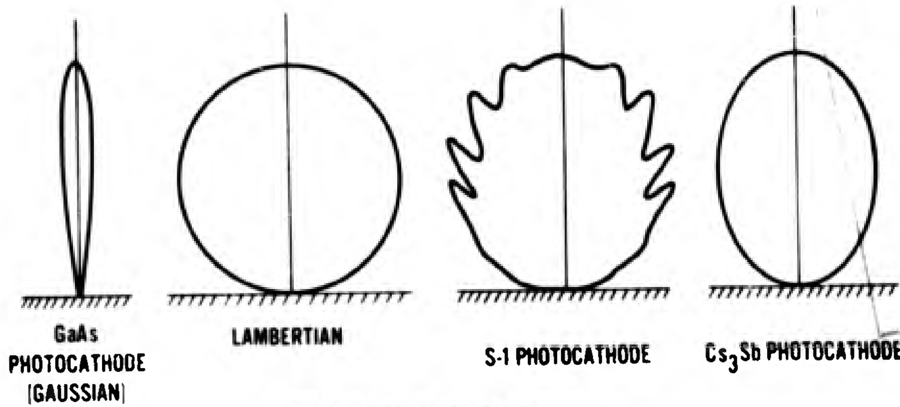

POLAR PLOTS OF DIFFERENTIAL YIELD

FIG. 10

End